npj | Quantum Materials

www.nature.com/npjquantmats

ARTICLE OPEN

c-axis pressure-induced antiferromagnetic order in optimally P-doped $BaFe_2(As_{0.70}P_{0.30})_2$ superconductor

Ding Hu[1,2], Weiyi Wang[2], Wenliang Zhang[3,4], Yuan Wei[3,4], Dongliang Gong[3,4], David W. Tam[2], Panpan Zhou[2], Yu Li[2], Guotai Tan[1], Yu Song[2], Robert Georgii[5], Björn Pedersen[5], Huibo Cao[6], Wei Tian[6], Bertrand Roessli[7], Zhiping Yin[1] and Pengcheng Dai[2]

Superconductivity in $BaFe_2(As_{1-x}P_x)_2$ iron pnictides emerges when its in-plane two-dimensional (2D) orthorhombic lattice distortion associated with nematic phase at T_s and three-dimensional (3D) collinear antiferromagnetic order at T_N ($T_s = T_N$) are gradually suppressed with increasing x, reaching optimal superconductivity around $x = 0.30$ with $T_c \approx 30$ K. Here we show that a moderate uniaxial pressure along the *c*-axis in $BaFe_2(As_{0.70}P_{0.30})_2$ spontaneously induces a 3D collinear antiferromagnetic order with $T_N = T_s > 30$ K, while only slightly suppresses T_c. Although a ~400 MPa pressure compresses the *c*-axis lattice while expanding the in-plane lattice and increasing the nearest-neighbor Fe–Fe distance, it barely changes the average iron-pnictogen height in $BaFe_2(As_{0.70}P_{0.30})_2$. Therefore, the pressure-induced antiferromagnetic order must arise from a strong in-plane magnetoelastic coupling, suggesting that the 2D nematic phase is a competing state with superconductivity.

npj Quantum Materials (2018)3:47 ; doi:10.1038/s41535-018-0122-3

INTRODUCTION

High-transition temperature superconductors (high-T_c) such as copper oxides and iron pnictides have plethora of electronic phases that emerge from their three-dimensional (3D) antiferromagnetic (AF) ordered parent compounds.[1–6] While the microscopic mechanism of such emergence remains elusive, it is generally believed that the formation of different phases results from a subtle balance among the spin, charge, lattice and orbital degrees of freedom. Therefore, by using an external probe such as pressure to tune this balance, one can manipulate different emergent electronic phases in high-T_c superconductors, and understand their relationship with superconductivity.

In the case of iron pnictides such as $BaFe_2(As_{1-x}P_x)_2$,[7,8] where the parent compound $BaFe_2As_2$ has a collinear AF order below T_N preceded by a tetragonal-to-orthorhombic lattice distortion at T_s with $T_s \geq T_N$ (Fig. 1a–c),[4–6] optimal superconductivity with $T_c \approx 30$ K emerges upon complete suppression of the 3D AF order and T_s by increasing x to 0.3[9,10] or hydrostatic pressure.[11–13] From transport, magnetic penetration depth, and heat capacity measurements, a quantum critical point (QCP), where a nonzero temperature phase transition is suppressed continuously to zero temperature, has been identified near $x \approx 0.3$.[10] Although initial nuclear magnetic resonance (NMR) measurements[14] suggest that the observed QCP arises from the gradual suppression of the collinear AF order near $x = 0.3$, neutron diffraction and recent NMR measurements indicate that the AF transition in $BaFe_2(As_{1-x}P_x)_2$ disappears in a weakly first-order fashion near optimal superconductivity with an avoided magnetic QCP.[15–17] On the other hand, a two-dimensional (2D) nematic phase, whose electronic properties break the in-plane rotational symmetry but preserve the translational symmetry of the underlying lattice,[18] has been theoretically postulated below T_s[19–21] and experimentally observed in different families of iron pnictides.[22–27] In particular, elastoresistivity measurements in $BaFe_2(As_{1-x}P_x)_2$ reveal a diverging nematic susceptibility near $x \approx 0.3$, suggesting a nematic origin for the observed QCP.[28,29]

Although optimal superconductivity can be achieved by a continuous suppression of the finite temperature structural phase transition T_s and magnetic phase transition T_N to zero temperature through increasing P-doping in $BaFe_2(As_{1-x}P_x)_2$ (Fig. 1a-c),[9] it is rather difficult to study the interplay between the nematic/magnetic order and superconductivity due to the sensitive P-doping dependence of structural and magnetic transitions near the optimal superconductivity.[10] Therefore, it is unclear if the nematic phase, which is associated with T_s, help or compete with superconductivity. Although it has been argued theoretically that nematic fluctuations can enhance superconductivity,[30,31] the relationship between static nematic order and superconductivity is still unclear.

One way to resolve this problem is to use uniaxial pressure (strain) as a probe to tune the system toward or away from the optimal superconductivity. In general, T_c in iron based superconductors is related with crystal structural parameters including the height of As/P anion (pnictogen) to the Fe layer $h_{anion} = h_{As/P}$ (Fig. 1d).[32–36] For $BaFe_2(As_{1-x}P_x)_2$, increasing P-doping concentration is linearly associated with decreasing pnictogen height $h_{As/P}$, and reaches optimal superconductivity with $T_c \approx 30$ K near $h_{As/P} \approx 1.30$ Å (Fig. 1d).[37] From pressure dependence of thermodynamic measurements, it was found that a *c*-axis uniaxial pressure on $BaFe_2(As_{1-x}P_x)_2$ corresponds to an increased P-doping level.[11,38,39] This means that in the P underdoped regime ($x < 0.3$), uniaxial pressure along the *c*-axis will increase T_c and suppress T_N, while in

[1]Center for Advanced Quantum Studies and Department of Physics, Beijing Normal University, Beijing 100875, China; [2]Department of Physics and Astronomy, Rice University, Houston, TX 77005-1827, USA; [3]Beijing National Laboratory for Condensed Matter Physics, Institute of Physics, Chinese Academy of Sciences, Beijing 100190, China; [4]University of Chinese Academy of Sciences, Beijing 100049, China; [5]Heinz Maier-Leibnitz Zentrum, Technische Universität München, D-85748 Garching, Germany; [6]Neutron Scattering Division, Oak Ridge National Laboratory, Oak Ridge, TN 37831, USA and [7]Laboratory for Neutron Scattering and Imaging, Paul Scherrer Institut, CH-5232 Villigen, Switzerland
Correspondence: Ding Hu (dinghu@rice.edu) or Zhiping Yin (yinzhiping@bnu.edu.cn) or Pengcheng Dai (pdai@rice.edu)

Received: 19 March 2018 Revised: 28 August 2018 Accepted: 30 August 2018
Published online: 18 September 2018

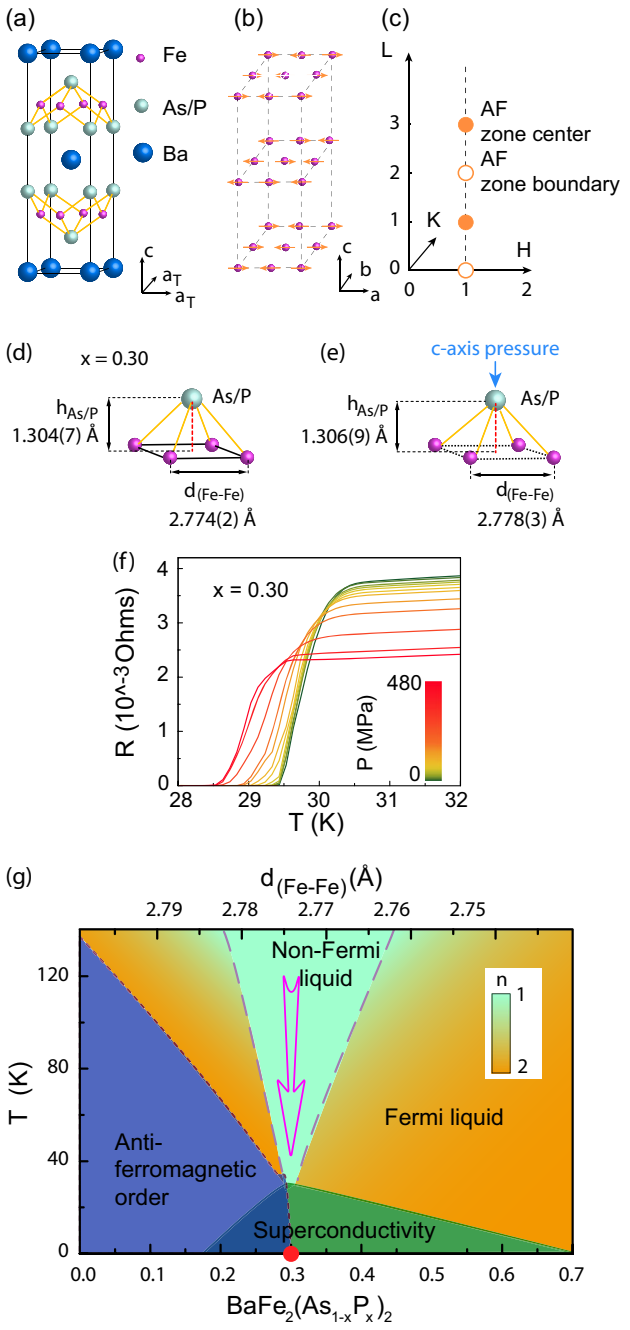

Fig. 1 Summary of the electronic phase diagram and uniaxial pressure effect on transport data in $BaFe_2(As_{1-x}P_x)_2$. **a** The crystal structure of $BaFe_2(As_{1-x}P_x)_2$. The purple, silvery, and blue balls indicate Fe, As/P, and Ba positions, respectively. **b** The collinear AF structure of $BaFe_2As_2$, which requires orthorhombic lattice distortion. **c** The corresponding reciprocal space, where AF Bragg peaks occur at (1, 0, *L*) with $L = 1, 3, \ldots$. **d** Schematic diagrams of the FeAs tetrahedron, showing the (As, P) height to iron plane is $h_{As/P} = 1.304(7)$ Å and the nearest in plabe Fe–Fe atom distance is 2.774(2) Å, respectively, for $BaFe_2(As_{0.70}P_{0.30})_2$ in 300 K. **e** By applying a uniaxial pressure along the *c*-axis, pnictogen height is $h_{As/P} = 1.306(9)$ Å and the in-plane Fe–Fe atom distance increases to 2.778(3) Å correspondingly. **f** Temperature dependence of in-plane resistance for pressures up-to 480 MPa along the *c*-axis of $BaFe_2(As_{0.70}P_{0.30})_2$ crystal. **g** The electronic phase diagram of $BaFe_2(As_{1-x}P_x)_2$, where AF, superconductivity, Fermi liquid, Non-Fermi liquid, and a QCP (red dot) are marked. The yellow and green colors represent the values of *n* in temperature dependence of the resistivity exponent.[10] Arrow marks the position in the phase diagram of the compound measured in this work

the overdoped regime without static AF order ($x \geq 0.3$), it will simply suppress T_c (Fig. 1e, f). Since nematic order in iron pnictides occurs below T_s,[21] a *c*-axis aligned uniaxial pressure on the tetragonal structured $BaFe_2(As_{0.70}P_{0.30})_2$ near the optimal superconductivity is not expected to induce static collinear AF order, which is associated with the in-plane orthorhombic lattice distortion (Fig. 1b). For $BaFe_2(As_{0.70}P_{0.30})_2$ near optimal superconductivity,[15,16] transport measurements at zero pressure revealed the linear temperature dependence of the resistivity above T_c [$R(T) = R(0) + aT^n$ with $n \approx 1$, where $R(T)$ is resistivity, a and n are fitting parameters.] (Fig. 1g).[10] Application of a *c*-axis pressure is expected to push the phase diagram into the overdoped regime, and should not alter dramatically the linear temperature dependence of the resistivity.

Surprisingly, we find that a *c*-axis aligned uniaxial pressure on $BaFe_2(As_{0.70}P_{0.30})_2$ not only suppresses T_c (Fig. 1f), but also induces resistivity deviation from the zero pressure linear temperature dependence (Fig. 2). Figure 3 shows uniaxial pressure dependence of T_c, suggesting an approximate linear relationship between the applied pressure and reduction in T_c below ~280 MPa. Upon further increasing uniaxial pressure, the reduction in T_c reduces, while the temperature where resistivity deviates from the linear temperature dependence increases (Fig. 3). Our neutron diffraction experiments on $BaFe_2(As_{0.70}P_{0.30})_2$ reveal that the deviation in resistivity from the linear temperature dependence in Figs. 2, 3 arise from a pressure-induced collinear AF order with $T_N > T_c$ (Figs. 4, 5). This is difficult to understand within the conventional Fermi surface nesting picture,[40] where a *c*-axis pressure is expected to induce pnictogen height reduction, promote electron itinerancy, and drive the system to the P-overdoped side with reduced T_c and no static AF order. Since the collinear AF order in iron pnictides has to be associated with the orthorhombic distortion of the underlying lattice (Fig. 1b),[3–6] our results provide the compelling evidence that a *c*-axis pressure actually induces an in-plane C_4 symmetry breaking field in the underlying lattice and drives the system into a nematic ordered phase. To understand this phenomenon, we carried out neutron diffraction experiments on single crystals with zero and ~400 MPa *c*-axis pressure. Our Rietveld analysis reveals that the dominant effect of a *c*-axis pressure is to suppress the *c*-axis and expand the in-plane lattice constants, and has limited effect on the average (As, P) pnictogen height $h_{As/P}$ (Fig. 1d, e, and Table 1). This is true even though As and P atoms occupy distinct positions in $BaFe_2(As_{1-x}P_x)_2$.[41] Based on the refined crystal structures at zero and finite pressure, we use a combination of density functional theory and dynamical mean field theory (DFT + DMFT)[42] to study the effect of a *c*-axis pressure on the magnetic property of $BaFe_2(As_{0.70}P_{0.30})_2$, and find that strong magnetoelastic coupling with the in-plane lattice is the driving force for the *c*-axis pressure induced the long-range static AF order. As the pressure-induced nematic order with T_N, $T_s > 30$ K increases with increasing pressure (Figs. 2–5), we conclude that the nematic order is competing with superconductivity and therefore needs to be taken into account to understand the electronic properties of iron pnictides.

RESULTS

Resistivity measurements

We chose to study the effect of a *c*-axis aligned uniaxial pressure on $BaFe_2(As_{0.70}P_{0.30})_2$ because P-substitution does not introduce significant disorder[43–45] and is expected to reduce the average pnictogen height linearly similar to *c*-axis applied pressure.[37]

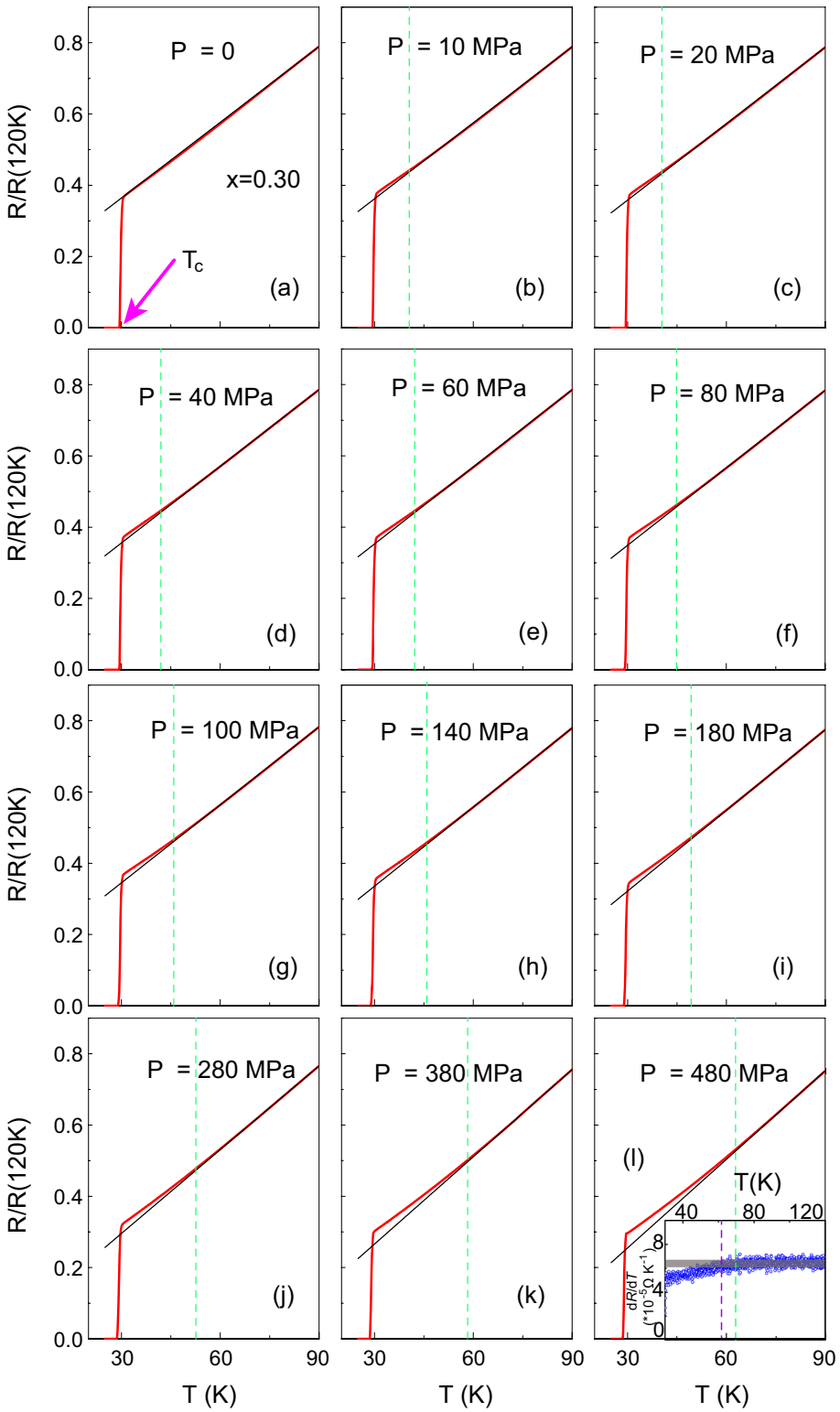

Fig. 2 Summary of pressure dependence of resistivity. Temperature dependence of normalized in-plane resistance for different pressures along the *c*-axis of $BaFe_2(As_{0.70}P_{0.30})_2$ crystal using automated uniaxial pressure device described in ref.[51]. **a** $P = 0$. The arrow indicates T_c at $\rho = 0$. **b** $P = 10$ MPa. **c** $P = 20$ MPa. **d** $P = 40$ MPa. **e** $P = 60$ MPa. **f** $P = 80$ MPa. **g** $P = 100$ MPa. **h** $P = 140$ MPa. **i** $P = 180$ MPa. **j** $P = 280$ MPa. **k** $P = 380$ MPa. **l** $P = 480$ MPa. The inset shows temperature derivative of the in-plane resistance, which reveals more clearly the deviation from linear temperature dependence. The black lines are the linear fits for high temperature data (80–120 K) and the vertical dashed green lines mark the temperature, where the observed resistance deviates from the linear temperature dependence

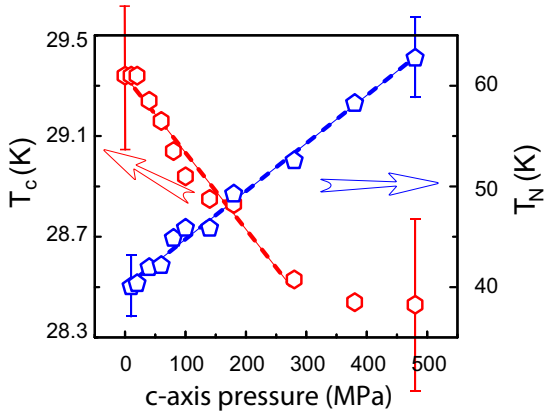

Fig. 3 The *c*-axis pressure dependence of T_c and T_N as determined from transport measurement. The *c*-axis uniaxial pressure dependence of T_c at $\rho = 0$ and the deviation temperatures from the linear temperature resistance. The error bars are the superconducting transition widths with $P_c = 0$ and 480 MPa. The error bars for T_N are estimated by using temperature derivative of the resistance data. The red and blue dashed lines are linear fits to the data

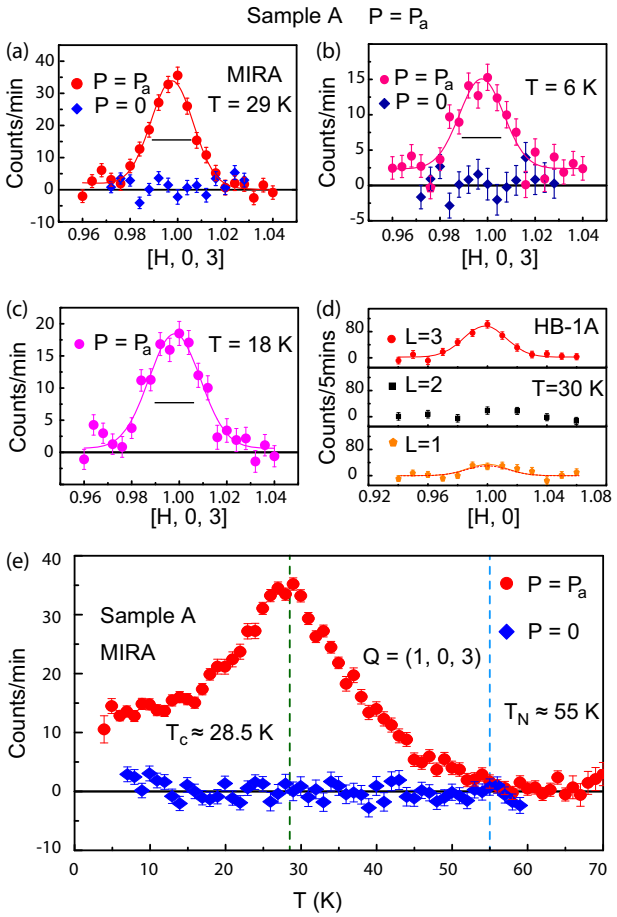

Fig. 4 Summary of neutron scattering results on sample A. The *c*-axis pressure-induced magnetic signal in sample A carried out at MIRA and HB-1A. **a**–**c** Wave vector scans through the (1, 0, 3) magnetic Bragg peak position at different temperatures with zero and finite pressure. The solid lines are Gaussian fits to the data, and the horizontal bars are instrumental resolution. **d** Wave vector scans along the [*H*, 0, *L*] direction with $L = 1$, 2, 3 at $T = 30$ K and finite pressure. **e** Temperature dependence of the magnetic scattering at $Q_{AF} = (1, 0, 3)$ for $P = P_a$ and P = 0. All shown data are background-corrected. All vertical error bars represent statistical error (1 s. d.)

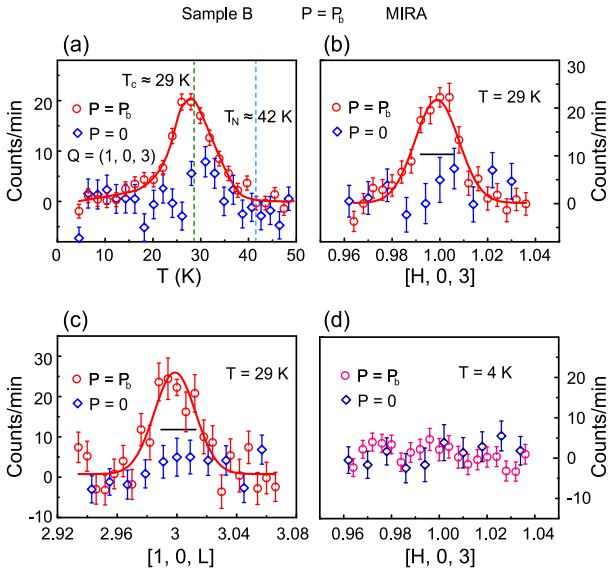

Fig. 5 Summary of neutron scattering results on sample B. Wave vector and temperature dependence of the uniaxial pressure induced magnetic order for sample B. **a** Temperature dependence of the magnetic scattering at (1, 0, 3) with and without pressure. **b**–**d** Wave vector scans along the [*H*, 0, 3] direction with and without uniaxial pressure at different temperatures. The absence of magnetic scattering at low-temperature (4 K) suggests that superconductivity can completely suppress the pressure induced magnetic order. The solid lines in **b** and **c** are Gaussian fits to the data, and the horizontal bars are instrumental resolution. The solid line in **a** is a guide to the eye. The blue and green vertical dashed lines in **a** mark T_N and T_c, respectively. All vertical error bars represent statistical error (1 s. d.)

Table 1. Results of single crystal diffraction experiments on sample A with $P = P_a$ and $P = 0$

	$a = b$	c	$d_{(Fe-Fe)}$	$z_{As/P}$	$h_{As/P}$
$P = 0$	5.548(4)	12.817(7)	2.774(2)	0.3517(5)	1.304(7)
$P = P_a$	5.556(6)	12.778(7)	2.778(3)	0.3522(7)	1.306(9)

The refined lattice constants, Fe–Fe distance, and $h_{As/P}$ of the $x = 0.30$ sample at 295 K

Previous transport measurements on $BaFe_2(As_{1-x}P_x)_2$ single crystals reveal that both the AF order and superconductivity are sensitive to the applied pressure.[39] Similar to other electron-doped iron pnictides,[46–50] in-plane uniaxial pressure that breaks the C_4 symmetry of the underlying lattice enhances the AF order and suppresses superconductivity in underdoped $BaFe_2(As_{1-x}P_x)_2$. For comparison, a *c*-axis aligned uniaxial pressure increases T_c and suppresses T_N in the underdoped regime, and is expected to only suppress T_c in the optimal/overdoped regime (Fig. 1g).[38,39] In addition, a *c*-axis pressure is also expected to expand the in-plane lattice parameter, akin to negative in-plane pressure.

We first describe *c*-axis pressure dependence of the resistivity on $BaFe_2(As_{0.70}P_{0.30})_2$. Figure 1f shows pressure dependence of the resistivity near T_c. With increasing pressure from 0 to 480 MPa using a custom designed uniaxial pressure device,[51] we see a systematic reduction in T_c from 29.5 to 28.5 K. Figure 2 summarizes temperature dependence of the resistivity as a function of increasing pressure. At zero pressure, we find linear temperature dependence of the resistivity above T_c and below 90 K, confirming previous work.[10] With increasing pressure from 0 to 480 MPa, temperature dependence of the resistivity systematically deviates

from the linear behavior as marked by the vertical green dashed lines in Fig. 2. This is reminiscent of the situation in $BaFe_2(As_{0.71}P_{0.29})_2$ at ambient condition, where the system orders antiferromagnetically at a temperature above T_c.[16] Assuming that the deviation from the linear temperature dependence is due to pressure-induced static AF order at T_N, we show in Fig. 3 pressure dependence of T_c and T_N. Simple linear fits to the data yield a reduction in T_c of 3.0 ± 0.2 K/GPa, and an increase of T_N of 48 ± 2 K/GPa if we ignore the $T_N = 0$ at zero pressure point (Fig. 3). From neutron diffraction experiments described below, we know that c-axis pressure-induced AF ordered moment in $BaFe_2(As_{0.70}P_{0.30})_2$ is vanishingly small compared with that of the parent compound $BaFe_2As_2$. Therefore, we do not expect a c-axis pressure will be able to induce observable magnetic ordered moment change in $BaFe_2As_2$.

Neutron scattering results

To confirm the results of transport measurements, we have carried out neutron diffraction experiments. Two single crystals of $BaFe_2(As_{0.70}P_{0.30})_2$, labeled A and B, were clamped between two Al plates using a pressure cell. We first carried out triple-axis measurements to determine the effect of uniaxial pressure on magnetic order. In order to determine the effect of c-axis uniaxial pressure on crystalline lattice, we measured many nuclear Bragg peaks in sample A after the triple axis measurements under pressure at room temperature. We then took another crystal from the same batch and put it in the identical pressure cell, and carried out the same diffraction measurement without pressure at room temperature. These two measurements allowed us to determine the effect of c-axis pressure on the atomic positions and lattice parameters of $BaFe_2(As_{0.70}P_{0.30})_2$.

Figure 4 summarizes the triple-axis neutron scattering results at zero and finite a c-axis uniaxial pressure on sample A. At zero pressure, the sample has no static AF order at $T = 29$ and 6 K as shown in wave vector scans along the [H, 0, 3] direction through the magnetic Bragg peak position at (1, 0, 3) (Fig. 4a, b). Upon application of a c-axis aligned uniaxial pressure P_a, we find temperature-dependent peaks at (1, 0, 3) (Fig. 4a–c). The solid lines in Fig. 4a–c are Gaussian fits to the data, which give the static spin–spin correlation lengths of 220 ± 30 Å, indicating pressure-induced long-range magnetic order. To determine the spin arrangements in the pressure-induced magnetic phase, we measured magnetic Bragg peaks at different L positions along the [H, 0] direction. Figure 4d shows wave vector scans along the [H, 0] direction at $L = 1$, 2, 3. For collinear AF order in underdoped $BaFe_2(As_{1-x}P_x)_2$, we expect magnetic Bragg peaks at $L = 1$, 3 and no magnetic scattering at $L = 2$.[4–6] Figure 4d shows that the magnetic scattering around (1, 0, 3) is about 3.1 times of that at (1, 0, 1), and no magnetic signal at (1, 0, 2). These results are consistent with the collinear AF order in underdoped $BaFe_2(As_{1-x}P_x)_2$.[16] By normalizing the magnetic Bragg peak intensity with a weak nuclear Bragg peak, we estimate that the pressure-induced magnetic ordered moment is about 0.1 μ_B/Fe. Figure 4e compares temperature dependence of the (1, 0, 3) scattering at zero ($P = 0$) and finite ($P = P_a$) c-axis pressure. While the scattering has no temperature dependence at zero pressure consistent with no magnetic order, its behavior at P_a is similar to those of underdoped $BaFe_2(As_{1-x}P_x)_2$ with $T_N \approx 55$ K, where the reduction of magnetic scattering below T_c is due to the competition of superconductivity with static AF order.[16]

Assuming that the temperature where resistivity deviates from the linear temperature dependence in c-axis pressured sample signals the start of static AF order, we compare T_N measured by neutron scattering in Figs. 3, 4 determined from transport measurements and find $P_a \approx 400$ MPa. The estimated P_a is consistent with the observed reduction in T_c as seen in magnetic scattering intensity reduction in Fig. 4e, although T_c of the sample can only be approximately determined by such measurement. To accurately determine the effect of c-axis uniaxial pressure on the pnictogen height $h_{As/P}$ and lattice parameters of $BaFe_2(As_{0.70}P_{0.30})_2$, we measured 30 Bragg peaks with $P = P_a$ and repeated the same measurement without pressure at room temperature using HB-3A four circle diffractometer. The Rietveld analysis of the single crystal diffraction data reveal that the major effect of a $P \approx 400$ MPa pressure is to suppress the c-axis and expand the in-plane lattice parameters without affecting much the average pnictogen height $h_{As/P}$ (Table 1).

To determine the uniaxial pressure dependence of the magnetic order, we carried out neutron scattering measurements on sample B under pressure $P = P_b < P_a$. Figure 5a shows temperature dependence of the magnetic scattering at (1, 0, 3) at zero and $P = P_b$. Similar to sample A, we find that uniaxial pressure induced magnetic order first appears below $T_N \approx 42$ K, competes with superconductivity below T_c, and is completely suppressed below 10 K. The lower T_N in sample B suggests $P_b \approx$ 40 MPa based on transport measurements in Fig. 3. Figure 5b–d compare zero and finite pressure ($P = P_b$) wave vector scans around (1, 0, 3) at different temperatures. From these scans, we estimate that pressure induced AF order has in-plane and c-axis spin–spin correlation lengths of about 120 and 160 Å, respectively. These results are consistent with those described in Fig. 4, revealing that a c-axis aligned uniaxial pressure spontaneously induces the collinear AF order with $T_N > 30$ K.

DFT + DMFT calculation

Our observation suggests that the magnetic properties of $BaFe_2(As_{0.70}P_{0.30})_2$ is very sensitive to small structure changes induced by the c-axis pressure at the optimal P-doping, signaling a large magnetoelastic coupling. Earlier DFT calculations[52] of the LaFeAsO parent compound revealed a strong dependence of the ordered magnetic moment on the As height. However, DFT calculations consistently overestimate the Fe ordered magnetic moment.[53] Although DFT + DMFT calculations can accurately reproduce the experimental ordered magnetic moments of Fe atoms in a large numbers of iron-based compounds with the same Hubbard U and Hund's coupling J as used in the current study,[53] the dependence of the Fe magnetic moment on the As height has not been carefully studied by DFT + DMFT calculations.

To determine the magnitude of the magnetoelastic coupling and understand the unusual behavior under c-axis pressure, we use a DFT + DMFT theory to study $BaFe_2(As_{0.70}P_{0.30})_2$.[42] In the DFT + DMFT calculations, the electronic charge was computed self-consistently on DFT + DMFT density matrix. The quantum impurity problem was solved by the continuous time quantum Monte Carlo method,[54,55] at a temperature of 72.5 K if not otherwise specified, and with a Hubbard $U = 5.0$ eV and Hund's rule coupling $J = 0.7$ eV in the AF state.[51,53,56] The experimental lattice constants of optimal P-doped $BaFe_2(As_{0.7}P_{0.3})_2$, $a = b = 5.5406$ Å and $c =$ 12.761 Å[8] are used in the calculations while the internal As/P position $z_{As/P}$ [where $h_{As/P} = (z_{As/P} - 0.25)c$] is varied from 0.349 to 0.347 in order to determine the (theoretical) critical As/P position/height. In the other set of calculations, the effect of c-axis pressure on the lattice is taken into account by expanding the in-plane lattice constant a by 1% and varying the internal As/P position in the same range whereas the c-lattice constant is fixed to the experimental value to simplify the computation since the As/P position/height and in-plane lattice constant are the dominating factors in determining the magnetic properties. By varying both the As/P height and the in-plane lattice constant, we are able to compute the magnitude of the in-plane and c-axis magnetoelastic coupling constants.

We summarize our DFT + DMFT results in Table 2. Keeping the lattice constant a and c unchanged and varying only the As/P height $z_{As/P}$ (second row in Table 2), the Fe ordered magnetic

Table 2. The DFT + DMFT calculated Fe ordered magnetic moment in the collinear AF state as a function of As/P height $z_{As/P}$ at the experimental and 1% expanded in-plane lattice constant while keeping the *c*-lattice constant unchanged

$z_{As/P}$	0.349	0.3485	0.348	0.3475	0.347
$\Delta a/a = 0$	0.138	0.065	<0.002	<0.001	<0.001
$\Delta a/a = 0.01$	0.217	0.143	0.049	0.002	<0.001

moment is 0.138 μ_B/Fe at $z_{As/P} = 0.349$, and quickly decreases to 0.065 μ_B/Fe at $z_{As,\ P} = 0.3485$, and less than 0.002 μ_B/Fe at $z_{As,\ P} = 0.348$. The Fe ordered magnetic moment changes at a rate of 11 μ_B/Å with the $h_{As/P}$, much larger than the corresponding value of ~3.7 μ_B/Å in LaFeAsO.[52] Therefore, the DFT + DMFT magnetoelastic coupling strength in optimal P-doped $BaFe_2(As_{1-x}P_x)_2$ is about 3 times stronger than the DFT magnetoelastic coupling strength in LaFeAsO, suggesting correlation-enhanced spin–phonon coupling.[57–59]

Keeping the (As, P) height unchanged at $z_{As/P} = 0.348$ as a function of increasing pressure, as seen experimentally in $BaFe_2(As_{0.70}P_{0.30})_2$ (Table 1), increasing the in-plane Fe–Fe spacing by 1% increases the Fe ordered moment to 0.049 μ_B/Fe, a change rate of 1.2 μ_B/Å, an order of magnitude smaller than the change rate with respect to the (As, P) height. Therefore, the (As, P) height is the dominating factor in the magnetic properties of the compound. This is further supported by the corresponding calculations at $z_{As/P} = 0.3475$ and 0.347 with experimental and 1% expanded in-plane lattice constant (Table 2). With slightly reduced $z_{As/P}$, expanding the in-plane Fe–Fe spacing by 1% barely increases the Fe ordered magnetic moment, in strong contrast to the results at $z_{As/P} = 0.348$. Therefore, the $z_{As/P} = 0.348$ is a critical (As, P) height where the Fe ordered magnetic moment is very sensitive to the in-plane Fe–Fe distance, similar to a previous observation that the Fe ordered magnetic moment shows a large enhancement under in-plane uniaxial pressure near an optimal superconductivity in $BaFe_{2-x}T_xAs_2$ (T = Co, Ni).[51]

Finally, we adopt the experimental results and carry out additional DFT + DMFT calculations in the AF state by expanding the in-plane lattice constant *a* by 0.5% (from 3.9178 Å to 3.9374 Å) and compressing the *c*-axis lattice constant by 1% (from 12.761 Å to 12.6347 Å) while the internal As/P position $z_{As/P}$ is changed from 0.348 to 0.349 in order to keep the As/P height unchanged. The calculations are done at a temperature of 29 K, below the experimental Néel temperature. We find that, without the *c*-axis pressure, the ordered Fe moment is still less than 0.01 μ_B, implying no long-range AF magnetic order. However, the long-range AF magnetic order emerges with an ordered Fe moment of 0.10 μ_B upon applying the aforementioned *c*-axis pressure. These findings are in good agreement with our experimental observation.

DISCUSSION

Our transport, neutron scattering experiments, and DFT + DMFT calculations on $BaFe_2(As_{0.70}P_{0.30})_2$ reveal that magnetism in this material is particularly sensitive to a *c*-axis-aligned uniaxial pressure. In previous transport, NMR, magnetic penetration depth, and heat capacity measurements, a QCP has been found at $BaFe_2(As_{0.70}P_{0.30})_2$.[10] In particular, differential elastoresistance measurements on $BaFe_2(As_{0.70}P_{0.30})_2$ indicate a diverging nematic susceptibility at $T = 0$, suggesting that the QCP is nematic in origin.[28] Since nematic fluctuations may enhance superconductivity,[30,31] it would be important to sort out the relationship between the static nematic phase and superconductivity.

In principle, nematic order of iron pnicitdes is an electronic anisotropic property of the 2D FeAs plane and should couple linearly to anisotropic strain (or pressure) within the FeAs plane in the limit of infinitesimal strains.[21] By measuring the rate of change of resistivity anisotropy with respect to the in-plane anisotropic strain, one can determine the nematic susceptibility.[28] By contrast, uniaxial pressure along the *c*-axis, which does not break the in-plane crystalline lattice symmetry, exhibits nonlinear coupling with the nematic order parameter.[60] Our surprising discovery that a *c*-axis aligned strain can actually induce AF order with in-plane symmetry-breaking field suggests that nematic order can also couple to the *c*-axis pressure via pressure-induced in-plane Fe–Fe distance expansion (Table 1). Although a ~400 MPa pressure along the *c*-axis suppresses the *c*-axis and expands the in-plane lattice parameters of $BaFe_2(As_{0.70}P_{0.30})_2$, it has negligible effect on the (As, P) height $h_{As/P}$ (Fig. 1d, e and Table 1). As demonstrated by our DFT + DMFT calculation, this means that $BaFe_2(As_{0.70}P_{0.30})_2$ is at critical doping regime with a critical As/P height where the Fe ordered moment and associated nematic order depend sensitively on the in-plane Fe–Fe distance. In the underdoped region, the As/P height is larger than the critical value of $h_{As/P} \approx 1.30$ Å and the long-range AF order already exists at ambient pressure. Applying a *c*-axis pressure does not change the AF order dramatically as it does at the optimal doping. On the other hand, in the overdoped region, where the As/P height is below the critical value, a *c*-axis pressure of similar magnitude should be unable to induce the long-range AF order as shown in Table 2. Further pressure-dependent transport and neutron scattering experiments as a function of P-doping will help us to better understand the quantum critical behavior in iron-based superconductors.

The *c*-axis pressure-induced AF order we observed in $BaFe_2(As_{0.70}P_{0.30})_2$ is in someways reminiscent of the effect of biaxial strain on the phase transitions in $Ca(Fe_{1-x}Co_x)_2As_2$.[61,62] Similar to *c*-axis uniaxial pressure, biaxial in-plane strain achieved by using the differential thermal expansion between the samples and a rigid substrate affects the *c*/*a* ratio of the tetragonal samples but does not break the tetragonal symmetry.[61] Instead of decreasing the *c*/*a* ratio by applying a *c*-axis pressure, biaxial in-plane strain in $Ca(Fe_{1-x}Co_x)_2As_2$ increases the *c*/*a* ratio and shifts the phase diagram of $Ca(Fe_{1-x}Co_x)_2As_2$ to higher *x*, without changing the maximum T_c and magnetic phase transition temperature.[61] Here, the quantum phase transition between the superconducting tetragonal and AF orthorhombic phases is first-order, and the resulting phase separation into these two phases with different in-plane lattice parameters allows the material to respond to biaxial strain in a continuous fashion.[62] For comparison with $BaFe_2(As_{0.70}P_{0.30})_2$, it would be interesting to experimentally determine the biaxial pressure dependence of the iron pnictogen height and Fe–Fe distance, and use DFT + DMFT calculation to see if the experimental phase diagram can be reproduced.

In summary, our neutron scattering results reveal that a moderate uniaxial pressure along the *c*-axis in $BaFe_2(As_{0.70}P_{0.30})_2$ superconductor can spontaneously induce a three-dimensional stripe AF order with $T_N > 30$ K, while only slightly suppresses T_c. These results indicate a strong magnetoelastic coupling near optimal superconductivity, suggesting a uniaxial pressure-induced nematic phase and stripe AF order competing with superconductivity in $BaFe_2(As_{1-x}P_x)_2$. These results are also consistent with zero pressure temperature dependence of neutron Larmor diffraction measurements on $NaFe_{1-x}Ni_xAs$, where the local orthorhombic lattice distortions associated with nematic phase were found to compete with superconductivity.[63]

METHOD

Single crystals of $BaFe_2(As_{0.70}P_{0.30})_2$ were prepared using self-flux method.[16] Transport measurements were carried out using a commercial physical property measurement system (PPMS) with the standard four-probe method (see Supplementary Information for device used in resistivity measurements). Our neutron scattering experiments were carried out using the MIRA triple-axis spectrometer at Maier–Leibnitz,

Garching, Germany,[64,65] HB-1A triple-axis spectrometer and HB-3A four circle diffractometer at High Flux Isotope Reactor, Oak Ridge National Laboratory (see Supplementary Information for the description of pressure cell used in neutron scattering experiments and addition data measured on HB-3A). We define the wave vector Q in three-dimensional reciprocal space in $Å^{-1}$ as $Q = Ha^* + Kb^* + Lc^*$, where H, K, and L are Miller indices and $a^* = \hat{a}2\pi/a$, $b^* = \hat{b}2\pi/b$, $c^* = \hat{c}2\pi/c$ are reciprocal lattice units (r.l.u.). In the low-temperature AF orthorhombic phase of $BaFe_2(As_{1-x}P_x)_2$, $a \approx 5.57$ Å, $b \approx 5.55$ Å, and $c \approx 12.80$ Å.[15] In this notation, we expect magnetic Bragg peaks of the collinear AF structure to occur at (1, 0, L) with $L = 1, 3, 5$ positions.[4–6] Near optimal superconductivity, the sample is a tetragonal paramagnet with $a = b$. Details of DFT + DMFT calculations are described in the Supplementary Information for additional data and analysis.

DATA AVAILABILITY

The data that support the findings of this study are available from the corresponding authors on request.

ACKNOWLEDGEMENTS

The neutron scattering work at Rice is supported by the U.S. NSF-DMR-1700081 (P.D.). A part of the material synthesis work at Rice is supported by the Robert A. Welch Foundation Grant no. C-1839 (P.D.). Z.Y. was supported by the NSFC (Grant no. 11674030), the Fundamental Research Funds for the Central Universities (Grant no.310421113) and the National Key Research and Development Program of China through Contract no. 2016YFA0302300. The calculations used high performance computing clusters at Beijing Normal University in Zhuhai and the National Supercomputer Center in Guangzhou. The work at IOP is supported by the "Strategic Priority Research Program (B)" of Chinese Academy of Sciences (XDB07020300), MOST (2012CB821400, 2011CBA00110,2015CB921302,2016YFA0300502), and NSFC (Nos. 11374011, 11374346, 91221303, 11421092, and 11574359). This research used resources at the High Flux Isotope Reactor, a DOE Office of Science User Facility operated by the Oak Ridge National Laboratory.

AUTHOR CONTRIBUTIONS

Most of the single crystal growth and neutron scattering experiments were carried out by D.H. with assistance from W.W., W.Z., Y.W., D.G., Y.S., R.G., B.P., H.C., W.T., and B. R. Transport measurements were carried out at Rice with the help from D.W.T. and P. P.Z. DFT + DMFT calculations are carried out by Z.Y. P.D. provided the overall lead of the project. The paper was written by H.D., Z.Y., and P.D. All authors provided comments.

ADDITIONAL INFORMATION

Supplementary information accompanies the paper on the *npj Quantum Materials* website (https://doi.org/10.1038/s41535-018-0122-3).

Competing interests: The authors declare no competing interests.

REFERENCES

1. Keimer, B., Kivelson, S. A., Norman, M. R., Uchida, S. & Zaanen, J. From quantum matter to high-temperature superconductivity in copper oxides. *Nature* **518**, 179–186 (2015).
2. Hosono, H. & Kuroki, K. Iron-based superconductors: current status of materials and pairing mechanism. *Phys. C Supercond. its Appl.* **514**, 399–422 (2015).
3. de la Cruz, C. et al. Magnetic order close to superconductivity in the iron-based layered $LaO_{1-x}F_xFeAs$ systems. *Nature* **453**, 899 (2008).
4. Huang, Q. et al. Neutron-diffraction measurements of magnetic order and a structural transition in the parent $BaFe_2As_2$ compound of FeAs-based high-temperature superconductors. *Phys. Rev. Lett.* **101**, 257003 (2008).
5. Kim, M. G. et al. Character of the structural and magnetic phase transitions in the parent and electron-doped $BaFe_2As_2$ compounds. *Phys. Rev. B* **83**, 134522 (2011).
6. Dai, P. Antiferromagnetic order and spin dynamics in iron-based superconductors. *Rev. Mod. Phys.* **87**, 855–896 (2015).
7. Stewart, G. R. Superconductivity in iron compounds. *Rev. Mod. Phys.* **83**, 1589–1652 (2011).
8. Johnston, D. C. The puzzle of high temperature superconductivity in layered iron pnictides and chalcogenides. *Adv. Phys.* **59**, 803–1061 (2010).
9. Jiang, S. et al. Superconductivity up to 30 K in the vicinity of the quantum critical point in $BaFe_2(As_{1-x}P_x)_2$. *J. Phys. Condens. Matter* **21**, 382203 (2009).
10. Shibauchi, T., Carrington, A. & Matsuda, Y. A quantum critical point lying beneath the superconducting dome in iron pnictides. *Annu. Rev. Condens. Matter Phys.* **5**, 113–135 (2014).
11. Tomić, M., Valent, R. & Jeschke, H. O. Uniaxial versus hydrostatic pressure-induced phase transitions in $CaFe_2As_2$ and $BaFe_2As_2$. *Phys. Rev. B* **85**, 094105 (2012).
12. Yamazaki, T. et al. Appearance of pressure-induced superconductivity in $BaFe_2As_2$ under hydrostatic conditions and its extremely high sensitivity to uniaxial stress. *Phys. Rev. B* **81**, 224511 (2010).
13. Duncan, W. J. et al. High pressure study of $BaFe_2As_2$—the role of hydrostaticity and uniaxial stress. *J. Phys. Condens. Matter* **22**, 052201 (2010).
14. Nakai, Y. et al. Unconventional superconductivity and antiferromagnetic quantum critical behavior in the isovalent-doped $BaFe_2(As_{1-x}P_x)_2$. *Phys. Rev. Lett.* **105**, 107003 (2010).
15. Allred, J. M. et al. Coincident structural and magnetic order in $BaFe_2(As_{1-x}P_x)_2$ revealed by high-resolution neutron diffraction. *Phys. Rev. B* **90**, 104513 (2014).
16. Hu, D. et al. Structural and magnetic phase transitions near optimal superconductivity in $BaFe_2(As_{1-x}P_x)_2$. *Phys. Rev. Lett.* **114**, 157002 (2015).
17. Dioguardi, A. P. et al. NMR evidence for inhomogeneous nematic fluctuations in $BaFe_2(As_{1-x}P_x)_2$. *Phys. Rev. Lett.* **116**, 107202 (2016).
18. Fradkin, E., Kivelson, S. A., Lawler, M. J., Eisenstein, J. P. & Mackenzie, A. P. Nematic fermi fluids in condensed matter physics. *Annu. Rev. Condens. Matter Phys.* **1**, 153–178 (2010).
19. Fang, C., Yao, H., Tsai, W.-F., Hu, J. & Kivelson, S. A. Theory of electron nematic order in LaFeAsO. *Phys. Rev. B* **77**, 224509 (2008).
20. Fernandes, R. M., Abrahams, E. & Schmalian, J. Anisotropic in-plane resistivity in the nematic phase of the iron pnictides. *Phys. Rev. Lett.* **107**, 217002 (2011).
21. Fernandes, R. M., Chubukov, A. V. & Schmalian, J. What drives nematic order in iron-based superconductors? *Nat. Phys.* **10**, 97–104 (2014).
22. Chu, J. H. et al. In-plane resistivity anisotropy in an underdoped iron arsenide superconductor. *Science* **329**, 824–826 (2010).
23. Tanatar, M. A. et al. Uniaxial-strain mechanical detwinning of $CaFe_2As_2$ and $BaFe_2As_2$ crystals: optical and transport study. *Phys. Rev. B* **81**, 184508 (2010).
24. Fisher, I. R., Degiorgi, L. & Shen, Z. X. In-plane electronic anisotropy of underdoped '122' Fe–arsenide superconductors revealed by measurements of detwinned single crystals. *Rep. Progress. Phys.* **74**, 124506 (2011).
25. Kasahara, S. et al. Electronic nematicity above the structural and superconducting transition in $BaFe_2(As_{1-x}P_x)_2$. *Nature* **486**, 382 (2012).
26. Lu, X. Y. et al. Nematic spin correlations in the tetragonal state of uniaxial-strained $BaFe_{2-x}Ni_xAs_2$. *Science* **345**, 657 (2014).
27. Rosenthal, E. P. et al. Visualization of electron nematicity and unidirectional antiferroic fluctuations at high temperatures in NaFeAs. *Nat. Phys.* **10**, 225–232 (2014).
28. Kuo, H. H., Chu, J. H., Palmstrom, J. C., Kivelson, S. A. & Fisher, I. R. Ubiquitous signatures of nematic quantum criticality in optimally doped Fe-based superconductors. *Science* **352**, 958 (2016).
29. Analytis, J. G. et al. Transport near a quantum critical point in $BaFe_2(As_{1-x}P_x)_2$. *Nat. Phys.* **10**, 194–197 (2014).
30. Metlitski, M. A., Mross, D. F., Sachdev, S. & Senthil, T. Cooper pairing in non-Fermi liquids. *Phys. Rev. B* **91**, 115111 (2015).
31. Lederer, S., Schattner, Y., Berg, E. & Kivelson, S. A. Enhancement of superconductivity near a nematic quantum critical point. *Phys. Rev. Lett.* **114**, 097001 (2015).
32. Zhao, J. et al. Structural and magnetic phase diagram of $CeFeAsO_{1-x}F_x$ and its relation to high-temperature superconductivity. *Nat. Mater.* **7**, 953 (2008).
33. Lee, C.-H. et al. Effect of structural parameters on superconductivity in fluorine-free $LnFeAsO_{1-y}$ (Ln = La, Nd). *J. Phys. Soc. Jpn.* **77**, 083704 (2008).
34. Kotegawa, H., Kawazoe, T., Sugawara, H., Murata, K. & Tou, H. Effect of uniaxial stress for pressure-induced superconductor $SrFe_2As_2$. *J. Phys. Soc. Jpn.* **78**, 083702 (2009).
35. Kuroki, K., Usui, H., Onari, S., Arita, R. & Aoki, H. Pnictogen height as a possible switch between high-T_c nodeless and low-T_c nodal pairings in the iron-based superconductors. *Phys. Rev. B* **79**, 224511 (2009).
36. Chen, X., Dai, P., Feng, D., Xiang, T. & Zhang, F.-C. Iron-based high transition temperature superconductors. *Natl. Sci. Rev.* **1**, 371–395 (2014).
37. Kasahara, S. et al. Evolution from non-Fermi- to Fermi-liquid transport via isovalent doping in $BaFe_2(As_{1-x}P_x)_2$ superconductors. *Phys. Rev. B* **81**, 184519 (2010).
38. Böhmer, A. E. et al. Thermodynamic phase diagram, phase competition, and uniaxial pressure effects in $BaFe_2(As_{1-x}P_x)_2$ studied by thermal expansion. *Phys. Rev. B* **86**, 094521 (2012).

39. Kuo, H. H. et al. Magnetoelastically coupled structural, magnetic, and superconducting order parameters in $BaFe_2$ $(As_{1-x}P_x)_2$. *Phys. Rev. B* **86**, 0134507 (2012).
40. Hirschfeld, P. J., Korshunov, M. M. & Mazin, I. I. Gap symmetry and structure of Fe-based superconductors. *Rep. Progress. Phys.* **74**, 124508 (2011).
41. Rotter, M., Hieke, Ch & Johrendt, D. Different response of the crystal structure to isoelectronic doping in $BaFe_2$ $(As_{1-x}P_x)_2$ and $(Ba_{1-x}Sr_x)Fe_2As_2$. *Phys. Rev. B* **82**, 014513 (2010).
42. Kotliar, G. et al. Electronic structure calculations with dynamical mean-field theory. *Rev. Mod. Phys.* **78**, 865–951 (2006).
43. Analytis, J. G., Chu, J. H., McDonald, R. D., Riggs, S. C. & Fisher, I. R. Enhanced Fermi-surface nesting in superconducting $BaFe_2(As_{1-x}P_x)_2$ revealed by the de Haas-van Alphen effect. *Phys. Rev. Lett.* **105**, 207004 (2010).
44. van der Beek, C. J. et al. Quasiparticle scattering induced by charge doping of iron-pnictide superconductors probed by collective vortex pinning. *Phys. Rev. Lett.* **105**, 267002 (2010).
45. E. Klintberg, L. et al. Chemical pressure and physical pressure in $BaFe_2(As_{1-x}P_x)_2$. *J. Phys. Soc. Jpn.* **79**, 123706 (2010).
46. Dhital, C. et al. Effect of uniaxial strain on the structural and magnetic phase transitions in $BaFe_2As_2$. *Phys. Rev. Lett.* **108**, 087001 (2012).
47. Dhital, C. et al. Evolution of antiferromagnetic susceptibility under uniaxial pressure in $Ba(Fe_{1-x}Co_x)_2As_2$. *Phys. Rev. B* **89**, 214404 (2014).
48. Song, Y. et al. Uniaxial pressure effect on structural and magnetic phase transitions in NaFeAs and its comparison with as-grown and annealed $BaFe_2As_2$. *Phys. Rev. B* **87**, 184511 (2013).
49. Man, H. R. et al. Electronic nematic correlations in the stress-free tetragonal state of $BaFe_{2-x}Ni_xAs_2$. *Phys. Rev. B* **92**, 134521 (2015).
50. Lu, X. Y. et al. Impact of uniaxial pressure on structural and magnetic phase transitions in electron-doped iron pnictides. *Phys. Rev. B* **93**, 134519 (2016).
51. Tam, D. W. et al. Uniaxial pressure effect on the magnetic ordered moment and transition temperatures in $BaFe_{2-x}T_xAs_2$ (T=Co, Ni). *Phys. Rev. B* **95**, 060505(R) (2017).
52. Yin, Z. P. et al. Electron-hole symmetry and magnetic coupling in antiferromagnetic LaFeAsO. *Phys. Rev. Lett.* **101**, 047001 (2008).
53. Yin, Z. P., Haule, K. & Kotliar, G. Kinetic frustration and the nature of the magnetic and paramagnetic states in iron pnictides and iron chalcogenides. *Nat. Mater.* **10**, 932–935 (2011).
54. Haule, K. Quantum Monte Carlo impurity solver for cluster dynamical mean-field theory and electronic structure calculations with adjustable cluster base. *Phys. Rev. B* **75**, 155113 (2007).
55. Werner, P., Comanac, A., De' Medici, L., Troyer, M. & Millis, A. J. Continuous-time solver for quantum impurity models. *Phys. Rev. Lett.* **97**, 076405 (2006).
56. Yin, Z. P., Haule, K. & Kotliar, G. Magnetism and charge dynamics in iron pnictides. *Nat. Phys.* **7**, 294–297 (2011).
57. Yin, Z. P., Kutepov, A. & Kotliar, G. Correlation-enhanced electron–phonon coupling: applications of GW and screened hybrid functional to bismuthates, chloronitrides, and other high-T_c superconductors. *Phys. Rev. X* **3**, 021011 (2013).
58. Mandal, S., Cohen, R. E. & Haule, K. Strong pressure-dependent electron–phonon coupling in FeSe. *Phys. Rev. B* **89**, 220502(R) (2014).
59. Gerber, S. et al. Femtosecond electron–phonon lock-in by photoemission and x-ray free-electron laser. *Science* **357**, 71 (2017).
60. Fujii, C. et al. Diverse fluctuations and anisotropic Gruneisen parameter behavior in iron-based superconductor $Ba(Fe_{1-x}Co_x)_2As_2$ and their correlation with superconductivity. *J. Phys. Soc. Jpn.* **1801**, 02791 (2018).
61. Böhmer, A. E. et al. Effect of biaxial strain on the phase transitions of $Ca(Fe_{1-x}Co_x)_2As_2$. *Phys. Rev. Lett.* **118**, 107002 (2017).
62. Fente, A. et al. Direct visualization of phase separation between superconducting and nematic domains in Co-doped $CaFe_2As_2$ close to a first-order phase transition. *Phys. Rev. B* **97**, 014505 (2018).
63. Wang, W. Y. et al. Local orthorhombic lattice distortions in the paramagnetic tetragonal phase of superconducting $NaFe_{1x}Ni_xAs$. *Nat. Commun.* **9**, 3128 (2018).
64. Georgii, R. & Seemann, K. MIRA: dual wavelength band instrument. *JLSRF*, 1, A3 (2015).
65. Georgii, R. et al. The multi-purpose three-axis spectrometer (TAS) MIRA at FRM II. Nuclear Instruments and Methods in Physics Research Section A: Accelerators, Spectrometers, Detectors and Associated Equipment 881, 60–64 (2018).